Journal of ELECTRONIC MATERIALS, Vol. 45, No. 7, 2016
DOI: 10.1007/s11664-016-4469-6
© 2016 The Minerals, Metals & Materials Society

CrossMark

Characterization of ZnO Thin Films Prepared by Thermal Oxidation of Zn

I. BOUANANE,[1] A. KABIR,[1,4,5] D. BOULAININE,[1] S. ZERKOUT,[2] G. SCHMERBER,[3] and B. BOUDJEMA[1]

1.—Laboratoire de Recherche sur la Physico-Chimie des Surfaces et Interfaces (LRPCSI), Faculté des Sciences, Université 20 août 1955-Skikda, B.P. 26, Route d'El-Hadaiek, 21000 Skikda, Algeria. 2.—LCC, Université de Constantine I, 25000 Constantine, Algeria. 3.—IPCMS, UMR 7504 CNRS-UdS, 23 rue du Loess, B.P. 43, 67034 Strasbourg Cedex 2, France. 4.—e-mail: a.kabir@univ-skikda.dz. 5.—e-mail: a.nour_kabir@yahoo.fr

Zinc oxide thin films were prepared by thermal oxidation of zinc films at a temperature of 500°C for 2 h. The Zn films were deposited onto glass substrates by magnetron RF sputtering. The sputtering time varied from 2.5 min to 15 min. The physico-chemical characterization of the ZnO films was carried out depending on the Zn sputtering time. According to x-ray diffraction, ZnO films were polycrystalline and the Zn-ZnO phase transformation was direct. The mean transmittance of the ZnO films was around 80% and the band gap increased from 3.15 eV to 3.35 eV. Photoluminescence spectra show ultraviolet, visible, and infrared emission bands. The increase of the UV emission band was correlated with the improvement of the crystalline quality of the ZnO films. The concentration of native defects was found to decrease with increasing Zn sputtering time. The decrease of the electrical resistivity as a function of Zn sputtering time was linked to extrinsic hydrogen-related defects.

Key words: ZnO, semiconductors, thin films, sputtering, luminescence, defects

INTRODUCTION

Among the transparent and conductive oxides (TCO), zinc oxide (ZnO) is a promising material for different applications in the optoelectronic field such as: transparent electrode in displays,[1] window layer in solar cells,[2] ultraviolet laser emission,[3] piezoelectricity,[4] bio-sensors,[5] short wavelength light emitting diodes and information technology.[6] This material is a *n*-type semiconductor and has a direct band gap of 3.37 eV at room temperature.[7] Because of its interesting properties, many works were focused on the elaboration of ZnO films by several methods such as magnetron sputtering,[8] molecular beam epitaxy,[9] chemical vapor deposition,[10] pulsed laser deposition (PLD),[11] chemical bath deposition (CBD),[12] spray pyrolysis,[13] sol–gel,[14] electrochemical deposition,[2] hydrothermal growth[15] and thermal decomposition.[16]

Another process to obtain ZnO films is the thermal oxidation of metallic Zn layers which takes advantage of its simplicity of the process. For example, ZnO thin films were obtained by thermal oxidation of ZnS thin films deposited by both chemical baths[17] and SILAR[18] methods and, also by thermal oxidation of Zn films deposited by vacuum evaporation method.[19] The optoelectronic properties of ZnO films attracted the interest of many researchers due to its above cited applications.[20,21] The luminescence mechanism in ZnO is still not well understood, in spite of the extensive experimental and theoretical works done before.[22–28] There is a big controversy as regards of the origin of the different emission bands.[29] This controversy is generally due to the presence of many defects emitted at the same time.[29] For the green emission around 516 nm, native defects (oxygen

(Received December 12, 2015; accepted March 18, 2016; published online April 19, 2016)

vacancies V_O[22,28] and zinc vacancies V_{Zn}[27]) and impurities[26] are considered to be at the origin of this emission. In addition to this green emission band, other emission bands are also observed.[30] A yellow emission band was detected in pulsed laser deposited ZnO[31] and in ZnO:Al prepared by solid-state reactions.[32] A red emission band was detected in spray pyrolysis deposited ZnO[33] and in ZnO single-crystals implanted, at 475°C, with Li, Na, N, P and Ne ions.[34]

These emissions are mainly due to native (or intrinsic) defects, including vacancies, interstitials and anti-sites. They considerably influence the optoelectronic properties of a semiconductor by affecting the doping charge carrier lifetime and the luminescence efficiency. Native defects have been invoked as sources of *n*-type conductivity in ZnO[35,36] since the intrinsic defects include also donor defects. However, it was found that these defects are not directly responsible for the unintentional *n*-type conduction in ZnO.[37]

In this work, we report on the fabrication of ZnO thin films by thermal oxidation of Zn deposited by RF magnetron sputtering. We report also on the investigation of the effect of Zn sputtering time on the structural an optoelectronic properties of ZnO films. The origin of UV, visible and infrared luminescence bands and the defects-related electrical conductivity will also be presented.

EXPERIMENTAL DETAILS

Zn thin films were first deposited by RF magnetron sputtering onto glass substrates under a pressure of 10^{-5} Torr. This pressure was reached by using a rotary pump and a diffusion pump successively. The sputtering target was a thick Zn disc of 99.9% purity and the target-substrate distance was about 8 cm. The AC power used for Zn target sputtering was kept at 100 W and the used frequency was 13.56 MHz. The magnetron cathode was used to increase the deposition rate. The Zn films of different thickness were obtained by varying the sputtering time from 2.5 min to 15 min. The Zn films were then annealed, in ambient air for 2 h, at a temperature of 500°C using a muffle furnace. Samples were pushed into the furnace when the temperature reaches the acquired value and pulled out quickly when oxidation is finished.

Several techniques were used to characterize the obtained oxide films for their structural, transmittance, photoluminescence and electrical properties. X-ray diffraction (XRD) was used to study the structural properties of the Zn oxidized films. The used diffractmeter was a Burker D8 Advanced equipped with an energy dispersive Sol-X detector and a $CuK_{\alpha1}$ radiation $\lambda = 0.154056$ nm source in the symmetric θ–2θ geometry ranging between 20° and 70°. The surface morphology of the oxide films was examined using a scanning electron microscope (SEM) operated at 3.0 kV. The samples for SEM were coated with a thin layer of carbon to reduce any charging effect. Optical transmittance spectra were recorded using a Perkin Elmer UV–Visible-NIR Lambda 950 spectrophotometer at room temperature in the wavelength range 350–900 nm. The photoluminescence (PL) spectra were acquired at room temperature with a 325-nm line of a frequency-tripled Nd-YAG laser as an excitation source. The electrical measurements were done using a Jandel four point probe connected to a Keithley 2400 source-meter.

RESULTS AND DISCUSSION

Figure 1 shows the XRD patterns for the Zn films, of different sputtering time, after oxidation at 500°C for 2 h. Miller indices are indicated on each diffraction peak. For all films, the hexagonal ZnO phase (wurtzite) is obtained from peaks located at about 31°, 34°, 36°, 47°, 56°, 62°, 67° and 69° corresponding respectively to (100), (002), (101), (102), (110), (103), (112) and (201) orientations (JCPDS 36-1451). From these diffraction peaks, one can deduce that an oxidation at 500°C for 2 h is sufficient to fully oxidize the sputtering deposited Zn films. Also, the Zn-ZnO phase transformation is direct whatever the Zn sputtering time. This is consistent with previous observations of ZnO films prepared by thermal oxidation of Zn.[38,39] For the Zn film deposited by sputtering for 2 min and 30 s, the amorphous XRD pattern, in spite of the presence of three small and narrow peaks corresponding to ZnO, is due to scattering by the glass substrate of the x-rays penetrating through the film. However, when the Zn sputtering time is increased, wurtzite peaks are observed in addition to the amorphous background of the glass substrate located between 20° and 40°. The peak intensity increased with the increasing Zn sputtering time indicating the high crystalline

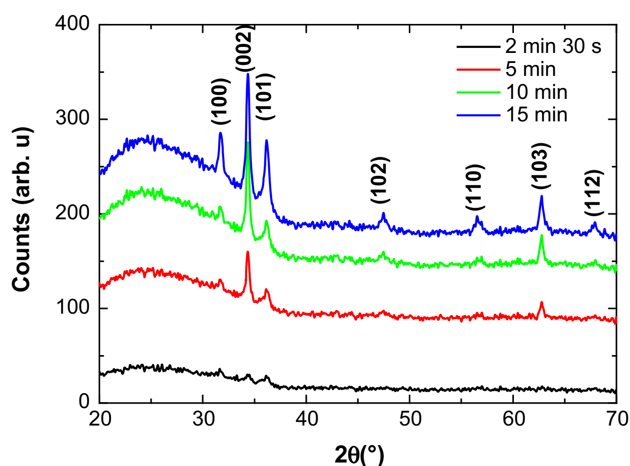

Fig. 1. XRD patterns of ZnO films obtained by thermal oxidation, at 500°C for 2 h, of Zn films. The Zn sputtering time varies from 2.5 min to 15 min.

quality of the formed ZnO films. The ZnO films were preferentially oriented along the (002) planes.

The (002)-oriented grain size D is presented, in Fig. 2, as a function of the Zn sputtering time. The increase of the grain size, as a function of the Zn sputtering time, reflects the improvement of the crystalline quality of ZnO (or completely oxidized Zn) films. The grain size of ZnO films was estimated using the Debye–Scherrer's formula neglecting peak broadening[40]:

$$D = \frac{0.9\lambda}{\beta \cos\theta} \quad (1)$$

where λ is the wavelength of the applied x-ray ($\lambda_{\text{Cu-K}\alpha1}$ = 0.154056 nm), θ is the Bragg's angle and β is the broadening of the diffraction line measured at half its maximum intensity in radians.

There is a clear difference between the growth of ZnO films deposited by other methods and their growth by the thermal oxidation of Zn films. The thermal oxidation method involves downward growth of ZnO from the ZnO surface to Zn-substrate interface[41] in contrast to the direct depositing methods where ZnO grows from the substrate upward.

The variation of the lattice constant c of ZnO films is shown, in the inset of Fig. 2, as a function of the Zn sputtering time. The lattice constants a and c can be calculated using the following equation:

$$\frac{1}{d_{hkl}^2} = \frac{3}{4}\left(\frac{h^2 + hk + k^2}{a^2}\right) + \frac{l^2}{c^2} \quad (2)$$

where h, k and l are the Miller indices. d_{hkl} is the lattice spacing calculated using the Bragg's equation. For calculation of the lattice constant c, we have used the peak position corresponding to (002) planes ($h = k = 0$ and $l = 2$), which reduces Eq. 2 to $c = 2d_{002}$.

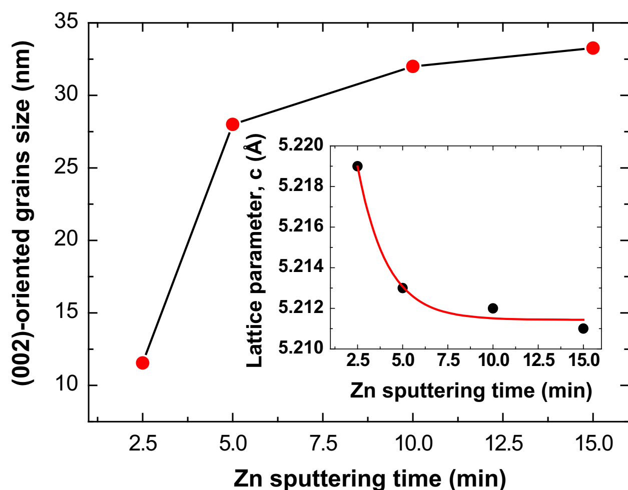

Fig. 2. (002)-oriented grain size in ZnO versus Zn sputtering time (Inset. The lattice parameter c versus Zn sputtering time).

The lattice constant c decreases, as a function of the Zn sputtering time, and then stabilizes from 5 min which indicates a relaxation of residual stress in ZnO films. The residual stress comprises thermal and intrinsic components.[42] The intrinsic stress may be induced by the growth parameters such as deposition temperature, applied power and pressure. It involved the creation of some defects like twins, precipitates, disoriented grains, grain boundaries and microcracks. A typical SEM image of ZnO film (Fig. 3) shows uniform deposited film without any above-cited defect. It has to be noticed that the grain size from SEM is a little bit bigger than that determined from XRD spectra using the Debye–Scherrer's formula. This may be due to the neglect of the peak broadening when using the Debye–Scherrer's formula.

Figure 4 shows optical transmittance spectra of ZnO films prepared by thermal oxidation of Zn deposited by sputtering at different times. All samples are transparent to the visible light, and the mean optical transmittance value was around 80%. The optical transmittance values depend on several factors such as thickness and defects. The interference fringes, observed in the visible region, confirm the uniformity of ZnO films. The rapid decrease of the transmittance, at the absorption edge, indicates a high crystalline quality of the films. One can observe that the absorption edge shifted toward lower wavelength with the increasing Zn sputtering time. This indicates a convergence of the energy band gap values to the bulk value (3.37 eV) may be caused by a decrease of lattice parameters. The ZnO film thickness d was estimated from the interference fringes using the following relation[43]:

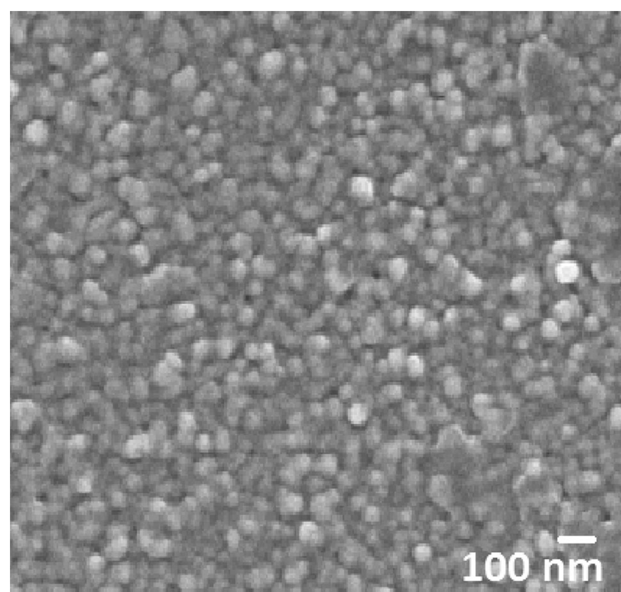

Fig. 3. Typical SEM image of ZnO surface obtained by thermal oxidation of Zn films.

$$d = \frac{\lambda_1 \times \lambda_2}{2[n_f(\lambda_1)\lambda_2 - n_f(\lambda_2)\lambda_1]} \quad (3)$$

where d is the film thickness and $n_f(\lambda_1)$ and $n_f(\lambda_2)$ are the refractive indices at λ_1 and λ_2 , respectively. The estimated thickness increases with the increasing Zn sputtering time, as shown in the inset of Fig. 4, from 194 nm to 653 nm. Because we have a complete transformation of Zn to ZnO, the thickness ratio for ZnO to Zn must be close to the volume ratio for wurtzite ZnO to Zn, i.e. 1.57.

The energy band gap values, as can be seen in Fig. 5, increase as a function of the Zn sputtering time from 3.15 eV to 3.35 eV and tend to converge toward the bulk ZnO value. These values are smaller than that of ZnO (3.37 eV); however, they are in good agreement with those reported in Refs. 44 and 45. The increase of the band gap energy can result from stress relaxation or defects decrease. For ZnO films, the variation of the absorption coefficient with the photon energy can be given by the following equation[46]:

$$\alpha h\upsilon = A(h\upsilon - E_g)^{1/2} \quad (4)$$

where α is the absorption coefficient, $h\upsilon$ is the photon energy, E_g is the optical band gap and A is a characteristic parameter independent of photon energy. The optical band gap (Fig. 5) is calculated by extrapolation of the linear part of $(\alpha h\upsilon)^2$, as a function of $h\upsilon$, to $\alpha h\upsilon = 0$ (inset of Fig. 5).

Figure 6 shows the dependence of room temperature photoluminescence (PL) spectra of ZnO films on Zn sputtering time. Each PL spectrum is characterized by a near-band-edge ultra-violet (UV) emission between 370 nm and 400 nm, a broad visible emission band extending from above 400 nm up to 750 nm and infrared (IR) emission located at about 765 nm.

The UV emission is originated from free-excitonic transitions.[9] The shift of the UV emission band to the highest energies indicates the enhancement of the band gap energy. In fact, both the UV emission band positions and the band gap energy calculated from the UV–visible spectra (Fig. 5) are close and comparable to the band gap of the bulk ZnO (3.37 eV). The increase of the intensity of the UV emission band between 370 nm and 400 nm (Fig. 6) reflects the amelioration of the crystalline quality of ZnO films according to Lee[47] in good agreement with what was deduced from the increase of the grain size and the diffraction peak intensity (see Figs. 1 and 2).

For the broad visible emission band (Fig. 6), two emission bands could be distinguished: a green emission band located at 520 nm and a red one at 700 nm. The intensity of these two bands decreases gradually with the increasing Zn sputtering time.

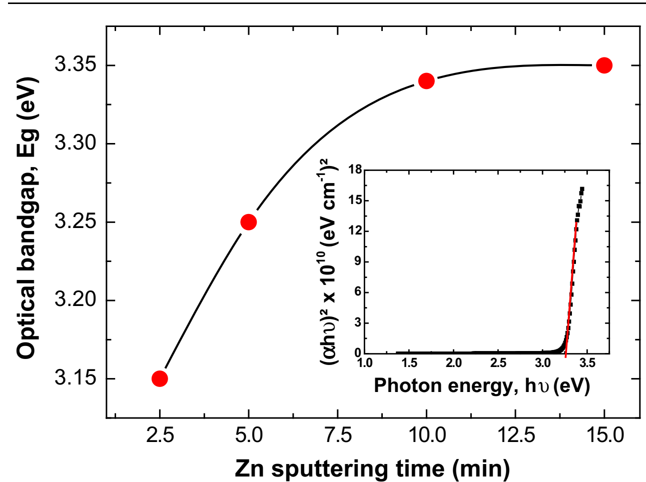

Fig. 5. Optical band gap as a function of Zn sputtering time (Inset. Plot of $(\alpha h\upsilon)^2$, as a function of $h\upsilon$).

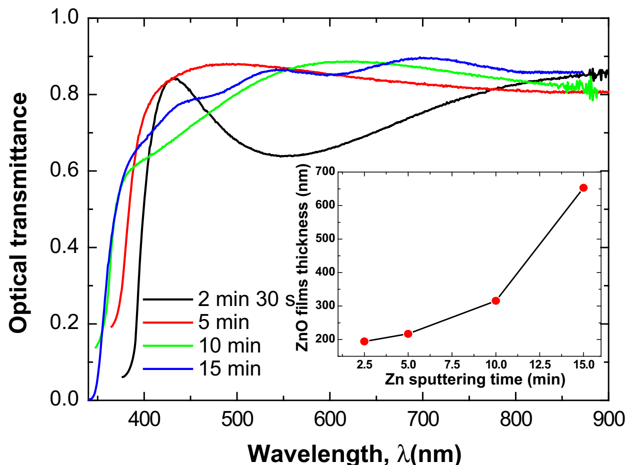

Fig. 4. Optical transmittance spectra of completely oxidized Zn films sputtered for different times (Inset. ZnO film thickness versus Zn sputtering time).

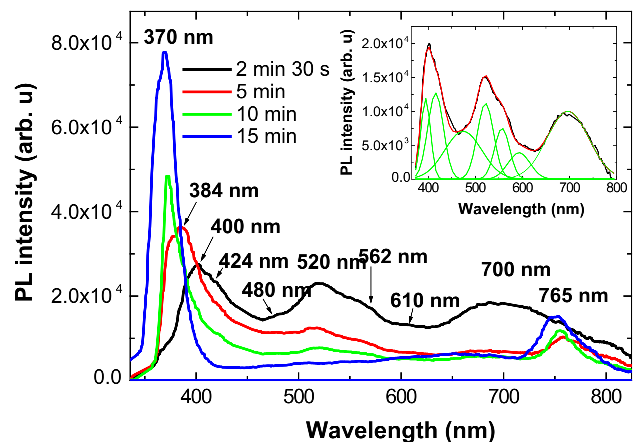

Fig. 6. PL spectra of completely oxidized Zn films deposited by RF magnetron sputtering for different times (Inset. Example of the decomposition of a PL spectrum).

The presence of the green and the red emission bands does not exclude the presence of other emission bands. The broadness of the visible emission band, in Fig. 6, results from the fact that it represents a superposition of many different deep levels emitting at the same time.

The visible emission band is generally composed of: a violet band around 410 nm attributed to Zn_i-valence band (VB) transition,[48] a blue band around 480 nm attributed to conduction band (CB)-V_{Zn} transition,[48] a green band around 520 nm attributed to CB-V_O transition,[49] a yellow band around 562 nm attributed to CB-O_i transition,[50] an orange band around 610 nm attributed to Zn_i-O_i transition[48] and a red band around 700 nm attributed to the lattice disorder along the c-axis due to Zn_i.[50] Another band located around 424 nm is attributed to hydrogen-related extrinsic defect (H-I or trapped OH^-).[51]

The native defect concentration N (per cm^3) in a crystal can be determined by using the Smakula's formula[52] given by:

$$N = 1.29 \times 10^{17} \frac{n}{f(n^2+2)^2} \alpha W_{1/2} \quad (5)$$

where n = 2 is the ZnO refractive index and f = 1 is the oscillator strength of the optical transmission. $W_{1/2}$ represents the width at half maximum of the PL band characterized by a maximum α.

A decomposition of the visible emission band into seven Gaussian peaks, based on the above bands positions, was done in order to replace the term $\alpha W_{1/2}$ in Eq. 5, by the Gaussian peak area corresponding to each native defect during calculus. An example of such a fitting is shown in the inset of Fig. 6.

Figure 7 shows the variation of the intrinsic defect concentration as a function of Zn sputtering time. We can see that the ZnO deep level concentration varies conversely with the Zn sputtering time. The decrease of the deep level concentration indicates the improvement of the ZnO film stoichiometry during the Zn-ZnO transformation induced by a thermal annealing at 500°C for 2 h.

The infrared (IR) emission band located at 765 nm is attributed, according to Manzano et al.,[53] to transition from oxygen interstitial (O_i) and oxygen anti-site (O_{Zn}) defects to the valence band. According to Yang,[54] the thermal annealing could be responsible for O_{Zn} defects following the reaction:

$$O_i + V_{Zn} \rightarrow O_{Zn} \quad (6)$$

The intensity of the IR emission band increases with the increasing Zn sputtering time (Fig. 6). This increase could be related to the increase of O_{Zn} defects. The decrease of the concentration of O_i and V_{Zn} defects, as a function of Zn sputtering time

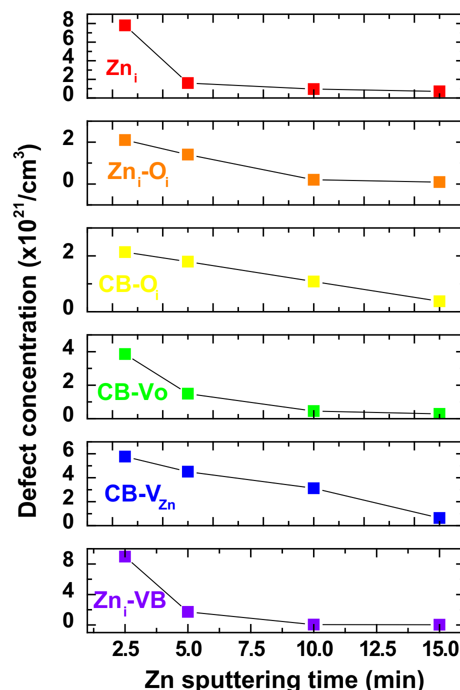

Fig. 7. Influence of Zn sputtering time on the native defect concentration formed in ZnO after thermal oxidation.

(Fig. 7), correlates with the increase of O_{Zn} defects, according to Eq. 6.

The variation of the electrical resistivity as a function of Zn sputtering time is shown in Fig. 8. We can see that the electrical resistivity decreases with the increasing Zn sputtering time. The decrease of the electrical resistivity is directly linked to the increase of the charge carriers, which depend on the donor-type defects concentration since ZnO is n-type semiconductor. Native defects are often considered as candidates to explain the n-type conductivity in ZnO. However, according to Janotti and Van de Walle,[37] these donor-defects are not responsible for n-type conductivity in ZnO. This correlates with our result since, as can be seen in Fig. 8, the above cited donor-defects concentration decreased as a function of the Zn sputtering time. Among the candidates to be a source of n-type conductivity in ZnO, hydrogen (H) impurities (noted H-I) have been proposed by Janotti and Van de Walle[37] as shallow donors. Their emission band is located at 424 nm in our PL spectra (see Fig. 6). The presence of hydrogen in our samples may result from the fact that sputtered Zn films were subjected to the ambient atmosphere for 6 days before oxidation and, according to Shi et al.,[55] hydrogen is stable in ZnO up to 500°C. To test the contribution of H-I defect in n-type conductivity, we have plotted, in Fig. 8, the evolution of their concentration, determined using Eq. 5, with the electrical resistivity as a function of Zn sputtering time. One can see that the H-I defects concentration increases when

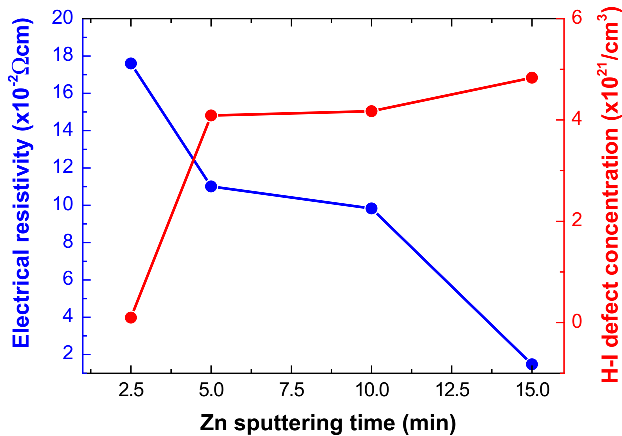

Fig. 8. Decrease of the electrical resistivity accompanied by the increase of the H-I defect concentration as a function of Zn sputtering time.

the electrical resistivity decreases. This may indicate that H-I defects directly contribute to the *n*-type conductivity of the investigated ZnO films. Hydrogen contribution in the increase in *n*-type conductivity was experimentally observed before by Lander[56] after the diffusion of H into ZnO and, by Baik et al.[57] after the proton implantation in ZnO followed by an annealing at 200°C. Other possible contributions in *n*-type conductivity are interfacial or depletion effects which are more important in thinner films and therefore produce a similar trend.

CONCLUSION

In this work, we found that physico-chemical properties of ZnO films, obtained by thermal oxidation of Zn at 500°C for 2 h, could be controlled by the Zn sputtering time. X-ray diffraction spectra showed that ZnO films were polycrystalline with a preferential orientation along the (002) planes. The absence of diffraction peaks linked to Zn or to other Zn-related phases indicated that the Zn-ZnO phase transformation was direct. The increase of the (002)-oriented grain size, as a function of Zn sputtering time, reflected the improvement of the crystalline quality of ZnO films. The investigated samples presented a high transmittance in the visible domain (around 80%). The interference fringes in the visible domain confirm the uniformity of the samples observed by the SEM technique. The optical band gap values ranged between 3.15 eV and 3.35 eV. These values were in good agreement with those reported by other teams for bulk ZnO. PL spectra of the investigated ZnO samples showed that they emitted in ultraviolet, visible and infrared. The increase of the ultraviolet emission band intensity, as a function of Zn sputtering time, was correlated to the improvement of the crystalline quality. The ultraviolet emission band coincided with the optical band gap values determined from the transmittance spectra. The intensity of the boarder visible emission band decreased with the increasing Zn sputtering time. The concentration of all native defects was found to decrease as a function of Zn sputtering time. The origin of infrared emission was confirmed to be the transition from O_i and O_{Zn} to the valence band. The increase of infrared emission band intensity was attributed to the increase of O_{Zn} defects. The electrical resistivity was observed to decrease with the increasing Zn sputtering time. Comparing this result to PL results, it has been deduced that the native donor-type defects (V_O, Zn_i and Zn_O) were not responsible for the *n*-type conduction in investigated samples. A correlation between the electrical resistivity and the extrinsic donor-type H-I defect concentration was established indicating that the H-I defects contribute to the *n*-type conduction in ZnO films. To measure the amount of hydrogen in the film and for the determination of the film density, nuclear techniques like elastic recoil detection analysis (ERDA) and Rutherford backscattering spectroscopy (RBS) should be used.

ACKNOWLEDGEMENTS

The authors gratefully acknowledge one of them, G. Schmerber, for the valuable discussions and for the structural and morphological characterization. Thanks are due to G. Ferblantier and D. Muller, from ICube in Strasbourg (France) for their help during the optical measurements.

REFERENCES

1. X. Jiang, F.L. Wong, M.K. Fung, and S.T. Lee, *Appl. Phys. Lett.* 83, 1857 (2003).
2. D. Gal, G. Hodes, D. Lincot, and H.W. Schock, *Thin Solid Films* 361–362, 79 (2000).
3. H. Fabricius, T. Skettrup, and P. Bisgaard, *Appl. Opt.* 25, 2764 (1986).
4. T. Yamamoto, T. Shiosaki, and A. Kawabata, *J. Appl. Phys.* 51, 3113 (1980).
5. T. Xu, G. Wu, G. Zhang, and Y. Hao, *Sens. Actuators A Phys.* 104, 61 (2003).
6. X. Li Guo, J.H. Choi, H. Tabata, and T. Kawai, *Jpn. J. Appl. Phys.* 40, 177 (2001).
7. Y.F. Chen, D.M. Bagnall, H.J. Koh, K.T. Park, K.J. Hiraga, Z.Q. Zhu, and T.F. Yao, *J. Appl. Phys.* 84, 3912 (1998).
8. X. Teng, H. Fan, S. Pan, C. Ye, and G. Li, *Mater. Lett.* 61, 201 (2007).
9. H.J. Ko, Y.F. Chen, Z. Zhu, T. Yao, I. Kobayashi, and H. Uchiki, *Appl. Phys. Lett.* 76, 1905 (2000).
10. F.G. Chen, Z.Z. Ye, W.Z. Xu, B.H. Zhao, L.P. Zhu, and J.G. Lv, *J. Cryst. Growth* 281, 458 (2005).
11. M. Hiramatsu, K. Imaeda, N. Horio, and M. Nawata, *J. Vac. Sci. Technol., A* 16, 669 (1998).
12. K. Govender, D.S. Boyle, P.B. Kenway, and P. O'Brien, *J. Mater. Chem.* 14, 2575 (2004).
13. R. Romero, D. Leinen, E.A. Dalchiele, J.R. Ramos-Barrado, and F. Martín, *Thin Solid Films* 515, 1942 (2006).
14. B.K. Choi, D.H. Chang, Y.S. Yoon, and S.J. Kang, *J. Mater. Sci. Mater. Electron.* 17, 1011 (2006).
15. S. Li, S. Zhou, H. Liu, Y. Hang, C. Xia, J. Xu, S. Gu, and R. Zhang, *Mater. Lett.* 61, 30 (2007).
16. Y. Yang, X. Li, J. Chen, H. Chen, and X. Bao, *Chem. Phys. Lett.* 373, 22 (2003).
17. E.J. Ibanga, C. Le Luyer, and J. Mugnier, *Mater. Chem. Phys.* 80, 490 (2003).

18. X.D. Gao, X.M. Li, and W.D. Yu, *Mater. Sci. Eng. B Solid-State Mater. Adv. Technol*. 113, 274 (2004).
19. S. Wang, G. Xia, J. Shao, and Z. Fan, *J. Alloys Compd.* 424, 304 (2006).
20. D.C. Look, *Mater. Sci. Eng.* 80, 383 (2001).
21. D.M. Bagnall, Y.F. Chen, Z. Zhu, T. Yao, S. Koyama, M.Y. Shen, and T. Goto, *Appl. Phys. Lett.* 70, 2230 (1997).
22. K. Vanheusden, W.L. Warren, C.H. Seager, D.R. Tallant, J.A. Voigt, and B.E. Gnade, *J. Appl. Phys.* 79, 7983 (1996).
23. D.C. Reynolds, D.C. Look, and B. Jogai, *J. Appl. Phys.* 89, 6189 (2001).
24. S.A. Studenikin and M. Cocivera, *J. Appl. Phys.* 91, 5060 (2002).
25. A. Van Dijiken, E.A. Meulenkamp, D. Vanmaekelbergh, and A. Meijerink, *J. Lumin.* 90, 123 (2000).
26. N.Y. Garces, L. Wang, L. Bai, N.C. Giles, L.E. Halliburton, and G. Cantwell, *Appl. Phys. Lett.* 81, 622 (2002).
27. A.F. Kohan, G. Ceder, D. Morgan, and C.G. Van de Walle, *Phys. Rev. B* 61, 15019 (2000).
28. S.B. Zhang, S.H. Wei, and A. Zunger, *Phys. Rev. B* 63, 075205 (2001).
29. A.B. Djurišić and Y.H. Leung, *Small* 2, 944 (2006).
30. Y.G. Wang, S.P. Lau, X.H. Zhang, H.W. Lee, S.F. Yu, B.K. Tay, and H.H. Hng, *Chem. Phys. Lett.* 375, 113 (2003).
31. X.L. Wu, G.G. Siu, C.L. Fu, and H.C. Ong, *Appl. Phys. Lett.* 78, 2285 (2001).
32. N. Ohashi, T. Nakata, T. Sekiguchi, H. Hosono, M. Mizuguchi, T. Tsurumi, J. Tanaka, and H. Haneda, *Jpn. J. Appl. Phys.* 38, 113 (1999).
33. S.A. Studenikin, N. Golego, and M. Cocivera, *J. Appl. Phys.* 84, 2287 (1998).
34. B.J. Pierce and R.L. Hengehold, *J. Appl. Phys.* 47, 644 (1976).
35. K.I. Hagemark, *J. Solid State Chem.* 16, 293 (1976).
36. G. Neumann, *Current Topics in Materials Science*, ed. E Kaldis (Amsterdam: North Holland, 1981).
37. A. Janotti and C.G. Van de Walle, *Rep. Prog. Phys.* 72, 126501 (2009).
38. N.H. Erdogan, K. Kara, H. Ozdamar, R. Esen, and H. Kavak, *Appl. Surf. Sci.* 271, 70 (2013).
39. I. Mihailova, V. Gerbreders, E. Tamanis, E. Sledevskis, R. Viter, and P. Sarajevs, *J. Non-Cryst. Solids* 377, 212 (2013).
40. B. Dennis, *Elements of X-ray Diffraction*, 3rd ed. (Upper Saddle River, NJ: Prentice-Hall International, 2000).
41. P. Kofstad, *High Temperature Corrosion* (London: Elsevier, 1988).
42. M. Wang, J. Wang, W. Chen, Y. Cui, and L. Wang, *Mater. Chem. Phys.* 97, 219 (2006).
43. R. Swanepoel, *J. Phys. E: Sci. Instrum.* 16, 1214 (1983).
44. M.F. El-Kuhaili, M.A. Al-Maghrabi, S.M.A. Durrani, and I.A. Bakhtiari, *J. Phys. D: Appl. Phys.* 41, 215302 (2008).
45. A.P. Rambu and G.I. Rusu, *Superlattice Microstr.* 47, 300 (2010).
46. J.I. Pankove, *Optical Processing in Semiconductors* (New York: Dover, 1971).
47. J.-H. Lee, *Electron. Mater. Lett*. 6, 155 (2010).
48. H.A. Ahn, Y.Y. Kim, D.C. Kim, S.K. Mohanta, and H.K. Cho, *J. Appl. Phys.* 105, 013502 (2009).
49. K. Vanheusden, C.H. Seager, W.L. Warren, D.R. Tallant, and J.A. Voigt, *Appl. Phys. Lett.* 15, 403 (1996).
50. D. Zwingel, *J. Lumin.* 5, 385 (1972).
51. E.V. Lavrov, J. Weber, C.G. Van de Walle, and R. Helbig, *Phys. Rev. B* 66, 165205 (2002).
52. C. Pollock, *J. Lumin.* 35, 65 (1986).
53. C.V. Manzano, D. Alegre, O. Caballero-Calero, B. Alén, and M.S. Martín-González, *J. Appl. Phys*. 110, 043538 (2011).
54. Y. Yang, H. Yan, Z. Fu, B. Yang, L. Xia, Y. Xu, J. Zuo, and F. Li, *Solid State Commun.* 138, 521 (2006).
55. G.A. Shi, M. Stavola, S.J. Pearton, M. Thieme, E.V. Lavrov, and J. Weber, *Phys. Rev. B* 72, 195211 (2005).
56. J.J. Lander, *J. Phys. Chem. Solids* 3, 87 (1957).
57. S.J. Baik, H.J. Jang, H.C. Lee, W.Y. Cho, and K.S. Lim, *Appl. Phys. Lett.* 70, 3516 (1997).